International Forum on Aeroelasticity and Structural Dynamics
IFASD 2017
25-28 June 2017 Como, Italy

AN INTEGRATED MODEL FOR LATERAL GUST LOADS ANALYSIS AND DUTCH ROLL FLIGHT DYNAMICS USING A 3D PANEL METHOD

Thiemo M. Kier[1]

[1]German Aerospace Center, DLR
Institute of System Dynamics and Control
82234 Weßling, GERMANY
Thiemo.Kier@dlr.de

Keywords: Loads Analysis, integrated flexible flight dynamics model, 3D Panel Methods, Aerodynamic Influence Coefficients, Lateral Gust, Dutch Roll.

Abstract: An integrated modelling approach for gust and manoeuvre loads analysis is presented. Typically, the unsteady aerodynamics for gust loads are computed by the Doublet Lattice Method. However, this method does not account for effects, which are important from a flight dynamics and manoeuvre loads perspective. E.g., the roll-yaw coupling, also responsible for the flight mechanical eigenmodes like the dutch roll mode, are unaccounted for by the DLM. Since, the dutch roll mode might also be excited by lateral gusts, this might have an influence on the loads response. In this paper, the unsteady aerodynamics are computed by a 3D panel method, capable of capturing the flight dynamics accurately and provide complex Aerodynamics Influence Coefficients for gust loads analysis as a function of reduced frequency similar to the DLM. The aerodynamics of the panel method are validate by comparison with CFD results. Differences in the flight mechanics between the DLM and the panel methods are assessed for a parametric variation of the wing dihedral of an aircraft model. Finally, results from a frequency domain gust loads analysis of a lateral gust for the DLM and the 3D panel method are compared.

1 INTRODUCTION

Maneuver and gust loads analysis are typically carried out, using different types of models to accommodate the specific needs of the involved disciplines. For maneuver loads analysis an accurate description of the flight dynamical behavior is essential. In particular, with respect to the flight mechanical modes, like phugoid, short period, spiral or dutch roll. Also nonlinearities in the aerodynamics over a certain range of angles of attack and large motions need to be considered. Since for large aircraft the motions during maneuvers are slow, a quasi-steady aerodynamics assumption is employed. For gust loads analysis on the other hand, the disturbances are small and linear equations of motion suffice. Unsteady aerodynamic effects however, are of major importance. These types of models are typically solved in the frequency domain, where unsteady aerodynamics based on linearized potential theory are conveniently available as a function of the reduced frequency parameter k by the use of the Doublet Lattice Method (DLM) [1–3]. A methodology how to integrate maneuver and gust simulations in a single loads analysis model is presented in [4].

However, ”classical” implementations of the DLM, respectively its quasi-steady counterpart the Vortex Lattice Method (VLM) [5], as used in popular aeroelastic solutions (e.g. in Nastran), do

not account for important effects. These implementations neglect forces acting in x-direction and hence any flight mechanical coupling of roll and yawing motion of the aircraft. In case of a lateral gust excitation, the rigid body dynamic response and hence the loads on the airframe might be altered significantly due to these coupling effects.

The 3D panel method NEWPAN [6] can capture these effects, as shown in [7, 8]. There, the steady Aerodynamic Influence Coefficient (AIC) matrices have been used to setup a so called AIC-ROM based on proper orthogonal decomposition (POD) for the use in manoeuvre loads applications. As mentioned earlier, for gust loads analysis, unsteady aerodynamic effects are no longer negligible, due to the rapid changes in onflow conditions compared to the relatively slow manoeuvre dynamics. The unsteady version of the 3D panel code, USNEWPAN, can also provide unsteady, complex valued AIC matrices as function of the reduced frequency.

This paper focuses on the use of these unsteady matrices for a lateral gust simulation, including flight mechanical effects, which are not present in methods like the DLM. First, a quick overview of the equations of motion of a loads analysis model for time and frequency simulations are presented. The underlying governing equations for the aerodynamic submodels of the DLM and 3D panel method are introduced and examples showing the validity of the panel method by comparison with Euler type CFD solutions are shown. Next, the contributing factors for the dutch roll mode are explained. A parametric study, which varies the geometric dihedral of an aircraft model is carried out. The differences between the DLM and the 3D panel method and the influence of these parameters on the dutch roll behavior are shown. Finally a frequency domain lateral gust analysis is presented and results are discussed.

2 LOADS ANALYSIS MODEL INTEGRATION

The following section describes the general principles regarding the integration aspects of the loads analysis model, i.e. the structural model, the equations of motion and the external forcing due to propulsion and the aerodynamics. These equations are integrated in the loads environment VarLoads [9] and are expressed in closed form by the use of AIC matrices, i.e. no iteration between the structural and the aerodynamic model is necessary.

2.1 Structural Dynamics, Equations of Motion and Load Recovery

The starting point, when setting up the equations of motion for a loads analysis model for a flexible aircraft is an Finite Element Model (FEM). This FEM usually consists of 100.000s of degrees of freedom (DoFs). Static condensation can be used to reduce the problem size by several orders of magnitude. The method employed is known as the Guyan reduction [10], where condensation points ($g-set$) are placed along a loads reference axes. The mass distributions are prepared for the corresponding payload/fuel cases and connected to the $g-set$. Subsequently a modal analysis is carried out and only part of the modal basis is retained to further reduce the model size and computational cost.

The eigenvalues and eigenvectors define the generalized coordinates of the $h-set$. The zero eigenvalues represent the rigid body motion. The $h-set$ can be partitioned into six rigid body DoFs ($b-set$) and flexible part ($f-set$). The rigid body mode shapes $\mathbf{\Phi}_{gb}$ and the retained modes of the eigenvector matrix $\mathbf{\Phi}_{gf}$ are used to generalized the equations of motion, which are given in the frequency domain by

$$\left\{-\omega^2 \begin{bmatrix} \mathbf{M}_{bb} & \mathbf{0} \\ \mathbf{0} & \mathbf{M}_{ff} \end{bmatrix} + \mathrm{j}\,\omega \begin{bmatrix} \mathbf{0} & \mathbf{0} \\ \mathbf{0} & \mathbf{B}_{ff} \end{bmatrix} + \begin{bmatrix} \mathbf{0} & \mathbf{0} \\ \mathbf{0} & \mathbf{K}_{ff} \end{bmatrix}\right\} \begin{bmatrix} \mathbf{u}_b \\ \mathbf{u}_f \end{bmatrix} = \begin{bmatrix} \mathbf{\Phi}_{gb}^{\mathrm{T}} \\ \mathbf{\Phi}_{gf}^{\mathrm{T}} \end{bmatrix} \mathbf{P}_g^{ext}(\omega). \qquad (1)$$

Note that the rigid body $b-set$ DoFs in (1) are defined in a earth fixed coordinate frame.

A suitable set of equations of motion to account for large rigid body motions and linear flexibility is derived in the references [11, 12]. The nonlinear equations of motion describe the movement relative to a "mean axes" body reference frame. Equations of motion for an unrestrained flexible aircraft accounting for large rigid body motions are given by

$$\begin{aligned} \begin{bmatrix} \mathbf{m}_b \left(\dot{\mathbf{V}}_b + \boldsymbol{\Omega}_b \times \mathbf{V}_b - \mathbf{T}_{bE}\, \mathbf{g}_E \right) \\ \mathbf{J}_b \dot{\boldsymbol{\Omega}}_b + \boldsymbol{\Omega}_b \times (\mathbf{J}_b \boldsymbol{\Omega}_b) \end{bmatrix} &= \boldsymbol{\Phi}_{gb}^{\mathrm{T}} \mathbf{P}_g^{\mathrm{ext}}(t) \\ \mathbf{M}_{ff} \ddot{\mathbf{u}}_f + \mathbf{B}_{ff} \dot{\mathbf{u}}_f + \mathbf{K}_{ff} \mathbf{u}_f &= \boldsymbol{\Phi}_{gf}^{\mathrm{T}} \mathbf{P}_g^{\mathrm{ext}}(t), \end{aligned} \tag{2}$$

where $\boldsymbol{\Phi}_{gb}$ is the rigid body modal matrix about the center of gravity and in directions as customary in flight mechanics, i.e x-forward, z-down. $\mathbf{V}_b$ and $\boldsymbol{\Omega}_b$ are the velocity, respectively angular velocity vectors in the body frame of reference. The matrix $\mathbf{T}_{bE}$ transforms the gravitational vector from an earth fixed (E) to the body fixed coordinate frame (b) as a function of Euler angles.

In order to recover the nodal loads $\mathbf{P}_g$ for a subsequent sizing of the structure, the force summation method (FSM) [13] is employed. Thus, subtraction of the inertial loads $\mathbf{P}_g^{\mathrm{iner}}$ from the external loads, yields

$$\mathbf{P}_g = \mathbf{P}_g^{\mathrm{ext}} - \underbrace{\mathbf{M}_{gg} \left\{ \boldsymbol{\Phi}_{gb}\, \ddot{\mathbf{u}}_b \quad + \quad \boldsymbol{\Phi}_{gf}\, \ddot{\mathbf{u}}_f \right\}}_{\mathbf{P}_g^{\mathrm{iner}}} \tag{3}$$

In the case of the nonlinear equations of motion (2), the rigid body acceleration is given as

$$\ddot{\mathbf{u}}_b = \begin{bmatrix} \dot{\mathbf{V}}_b + \boldsymbol{\Omega} \times \mathbf{V}_b - \mathbf{T}_{bE}\, \mathbf{g}_E \\ \dot{\boldsymbol{\Omega}}_b + \mathbf{J}_b^{-1} \left(\boldsymbol{\Omega}_b \times (\mathbf{J}_b \boldsymbol{\Omega}_b) \right) \end{bmatrix}. \tag{4}$$

The FSM requires the external forces to be available on the structural grid. This allows to accounts for the static part directly on the physical grid, and therefore has a good convergence behavior. Then cut loads can be computed by integrating the nodal loads along the loads reference axes of each aircraft component. The envelope of the cut loads is used as sorting criteria to obtain the critical load cases used for the structural sizing.

2.2 Aerodynamic Model

The major contribution to the external forces apart from the propulsion forces stem from the aerodynamics. So called Aerodynamic Influence Coefficient matrices based on linear potential flow theory have classically been used for aeroelastic applications.

2.2.1 Governing Flow Equations

The governing flow equations for the panel method as well as the DLM are the unsteady linearized potential flow equations, sometimes also referred to as the unsteady Prandtl-Glauert equations. The derivation of methods based on potential flow starts out with the steady velocity potential Φ_S.

$$\left(1 - M_\infty^2\right) \frac{\partial^2 \Phi_S}{\partial x^2} + \frac{\partial^2 \Phi_S}{\partial y^2} + \frac{\partial^2 \Phi_S}{\partial z^2} = 0 \tag{5}$$

Using a Göthert Type 2 transformation [14], the problem can be reduced to a Laplace type equation $\nabla^2 \Phi_S = 0$.

The Vortex Lattice Method (VLM) solves velocity potential equation by discretizing the mean lifting surface by so called horseshoe vortices, where the bound vortex lies on the quarter chord of ech box and the trailing vortices extend to infinity. The forces are the calulated by application of the Kutta Jokowsky Law, where the circulation is related to lift. In the case of the steady panel method the actual and not the mean surface is discretized. The basic solutions chosen are velocity potential source and doublet panels. The result is a velocity potential distribution. Differentiation of the this velocity potential in the spatial directions yield the flow velocities on the surface, which in turn can be used to determine the surface pressures and ultimately the lifting forces.

This steady solution about a, possibly deformed reference shape, defines the flight state about which an unsteady linearization is performed. The unsteady solution is then found by solving the linearized frequency domain variant of the unsteady Prandtl-Glauert equation

$$\left(1 - M_\infty^2\right) \frac{\partial^2 \Phi_U}{\partial x^2} + \frac{\partial^2 \Phi_U}{\partial y^2} + \frac{\partial^2 \Phi_U}{\partial z^2} - 2\mathrm{j}\omega \frac{M_\infty}{a_\infty} \frac{\partial \Phi_U}{\partial x} - \left(\frac{\omega^2}{a_\infty^2}\right) \Phi_U = 0, \tag{6}$$

where the unsteady potential is given as $\mathrm{e}^{\mathrm{j}\omega t}\ \Phi_U(x, y, z)$. This equation can be converted to a Helmholtz type equation

$$\nabla^2 \Phi_U + \kappa^2 \Phi_U = 0, \quad \text{with} \quad \kappa = k \frac{M_\infty}{1 - M_\infty^2}, \tag{7}$$

to determine the solution, where κ is a frequency parameter depending on the reduced frequency $k = \frac{c_{ref}/2}{U_\infty}\omega$ and Mach number.

The total velocity potential is then $\Phi(x, y, z, \omega) = \Phi_S(x, y, z) + \mathrm{e}^{\mathrm{j}\omega t}\ \Phi_U(x, y, z)$, In the case of the unsteady panel method, this expression is used to calculate the complex unsteady pressure via a linearized version of the unsteady Bernoulli equation. The Doublet Lattice Method (DLM) also provides a harmonic solution for equation (6), with some notable differences. The DLM uses the acceleration potential which is formally equivalent to the velocity potential equation. Therefore, the same elementary solutions are valid, e.g. the doublet potential. The acceleration potential readily yields the pressure difference between the upper and lower surface. Since there is no pressure jump across the wake, it can be omitted in the modeling process. Further due to the linearization applied in the derivation of the DLM, the coupling between the steady and unsteady flow is lost, which is accounted for by the 3D panel method intrinsically.

2.2.2 Aerodynamic Influence Coefficient Matrices and Boundary Conditions

Both described aerodynamic methods have in common the concept of the frequency dependent Aerodynamic Influence Coefficient (AIC) matrix. The AIC matrix relates a normal wash at a control point to a pressure at each of the discretization elements for discrete harmonic excitations in the frequency domain. When calulated over a range of reduced frequencies k, transfer functions relating normal wash excitations to pressures can be determined.

The pertubation pressures $\Delta\, \mathbf{c_p}$ about the steady state can be calculated with the following equation:

$$\Delta\, \mathbf{c_p}_j(k) = \left[\mathbf{Q}_{jj}\ \left(\mathbf{D^x}_{jk} + \mathrm{j}k \cdot\ \mathbf{D^t}_{jk}\right)\ + \left(\mathbf{DP^x}_{jk} + \mathrm{j}k \cdot\ \mathbf{DP^t}_{jk}\right)\right]\ \mathbf{u}_k(k), \tag{8}$$

where the matrix $\mathbf{D^x}_{jk}$ accounts for a change in downwash due to a change of the normal vector with respect to the free stream direction and the matrix $\mathbf{D^t}_{jk}$ for additional downwash due to movement of the boundary in direction of the panel normal. When thick bodies are modeled in potential flow, additional pressure contributions arise. These are not associated with the normalwash, but with tangential flow at the panels. Therefore, the 3D Panel Method, requires the additional motion induced terms $\mathbf{DP^x}_{jk}$ and $\mathbf{DP^t}_{jk}$. It should be noted that these terms are dependent on the onflow direction, i.e. they are associated with the flight state, about which the AIC was linearized. For thin velocity potential panels as well as in the DLM these terms are zero. The vector $\mathbf{u}_k(k)$ describes the motion of the individual panels at their reference point, which may result from rigid body motion, flexible deformation or control surface deflections.

If the excitation is not motion induced, but a result from atmospheric disturbances, the downwash due to these have to be determined in the frequency domain. E.g. the spectrum for a discrete tuned $\mathbf{v}_G(\omega)$ is available in a frequency dependent semi-analytically form with parameters like the gust gradient length. Further, when the aircraft is subjected to the gust, the penetration speed U_∞ and location of the control points $\mathbf{x}_j$ wrt the gust need to be considered. In the frequency domain these time lags are expressed as phase shifts with an exponential function.

$$\mathbf{w}_j^G(\omega) = \mathbf{n}_j \cdot \exp\left(-\mathrm{j}\omega \cdot \mathbf{x}_j/U_\infty\right) \cdot \mathbf{v}_G(\omega)/U_\infty \tag{9}$$

The dot product with $\mathbf{n}_j$ then determines the direction for vertical, lateral or head-on gusts.

2.2.3 Rational Function Approximation

The AIC matrices are tabulated values at discrete reduced frequencies. A Rational Function Approximation (RFA), where the frequency domain transfer functions are fit with suitable "rational" terms can be used to make them amendable for time domain integration. For rational functions, a Laplace transformation exists and therefore the unsteady aerodynamics can be cast in state space form. Many flavors of this method have been published in literature [15–18]. Fitting of the AICs $\mathbf{Q}_{jj}(k)$ without multiplication with differentiation matrices in eq. (8) has been proposed in [4]:

$$\mathbf{Q}_{jj}(\hat{s}) = \mathbf{Q^0}_{jj} + \mathbf{Q^1}_{jj}\hat{s} + \sum_{i=1}^{n_p} \mathbf{Q^{L}}_{i\,jj} \frac{\hat{s}\mathbf{I}}{\hat{s} + p_i}, \tag{10}$$

where $\hat{s} = s\left(\frac{c_{ref}/2}{U_\infty}\right)$ is the Laplace domain equivalent to the reduced frequency k. This "physical" RFA (10) has several advantages over the approximation of the generalized aerodynamic forces. E.g., the fit is not tied to a particular mass case and it allows to apply the time lags without approximation of the gust column. In the context of gust loads analysis, the RFA also allows evaluation in the frequency domain and constitutes another scheme for interpolation.

2.2.4 Pressure Integration and Grid Interpolation

The load transformation to panel reference point is done by integrating the pressures, which is mostly a simple multiplication with the aerodynamic box area. Depending on the method, an offset between force application location and the panel reference point may be present. The respective moment arms are accounted for by the integration matrix $\mathbf{S}_{kj}$, if rotational degrees of freedom are introduced in the aerodynamic $(k - set)$. Multiplication with the dynamic pressure yields the aerodynamic forces.

$$\mathbf{P}_k^{\text{aero}} = q_\infty \, \mathbf{S}_{kj} \, \mathbf{c}_{\mathbf{p}_j} \tag{11}$$

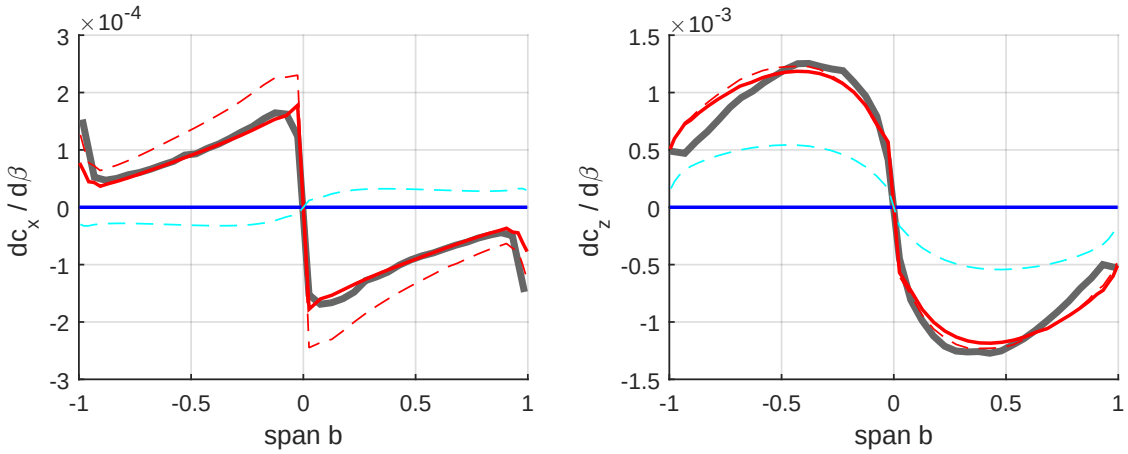

Figure 1: Drag, lift, and moment gradient distribution due β.

Finally, the aerodynamic loads have to be mapped to the structural degrees of freedom. The matrix connecting the displacements of the structural grid ($g-set$) to the aerodynamic grid ($k-set$) is called spline matrix $\mathbf{T}_{kg}$.

$$\mathbf{u}_k = \mathbf{T}_{kg}\mathbf{u}_g \tag{12}$$

This mapping is achieved, e.g. by employing radial basis functions, such as the commonly used Infinite Plate Spline (IPS) [19], or by using beam splines [20]. The physical interpretation is that the structure behaves plate or beam like and that the respective degrees of freedom sets $k-set$ and $g-set$ lie on the same structure described by the spline basis functions. The aerodynamic loads can be mapped back onto the structure with the transpose of the spline matrix, based on the principal of virtual work.

$$\mathbf{P}_g^{\text{aero}} = \mathbf{T}_{kg}^{\text{T}}\mathbf{P}_k^{\text{aero}} \tag{13}$$

2.3 Validation of the 3D panel method

To validate the results and demonstrate the capability to capture the flight mechanical effects, a comparison of the 3D panel method with the DLM and an CFD code solving Euler type governing equations is presented.

2.3.1 Quasi-steady lift distribution due to sideslip, yaw and roll rate

In [8] these comparisons were already presented in the light of a manoeuvre loads application. For the sake of completeness the results relevant for the dutch roll motion are repeated here. The chosen test case was the LANN wing [21]. The half wing was mirrored to obtain results for the lateral unsymmetric flow conditions. It has no dihedral and a cambered airfoil. To stay within the validity range of the governing equations of the potential flow the flight state was set at a subsonic Mach number of $Ma = 0.65$ and an angle of attack $\alpha = 0°$. Then spanwise lift distribution gradients due to beta, p and r were computed by simple finite differences for the CFD calculations. The distributions for the 3D panel were determined by multiplication of the steady ($k = 0$) AIC matrix with the corresponding boundary condition matrices, c.f. eq. (8).

The first effect to be examined is the rolling moment due to sideslip C_{L_β}. The perturbation step was $1°$ for the sideslip angle β. The panel method results show excellent correlation with the CFD results for all of the gradient distributions in drag and lift, depicted in figure 1. As expected

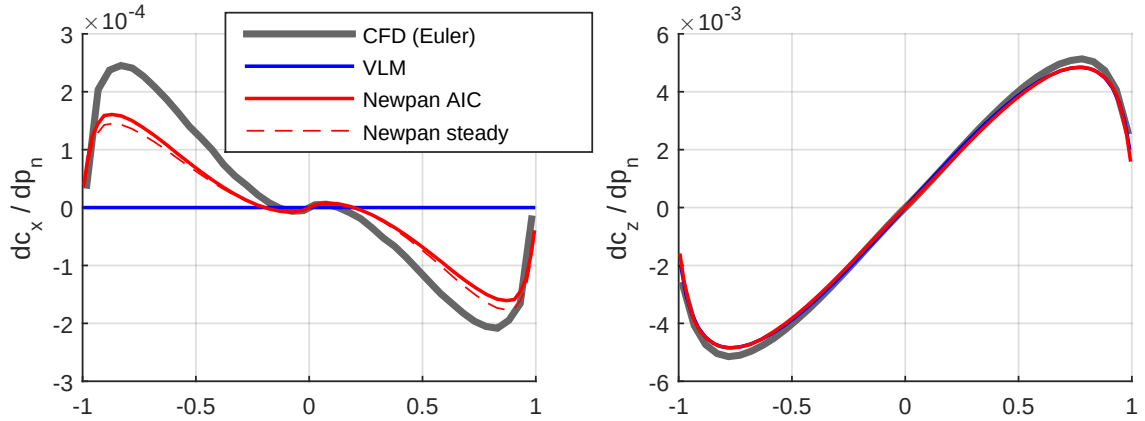

Figure 2: Drag and lift gradient distribution due roll rate p_n.

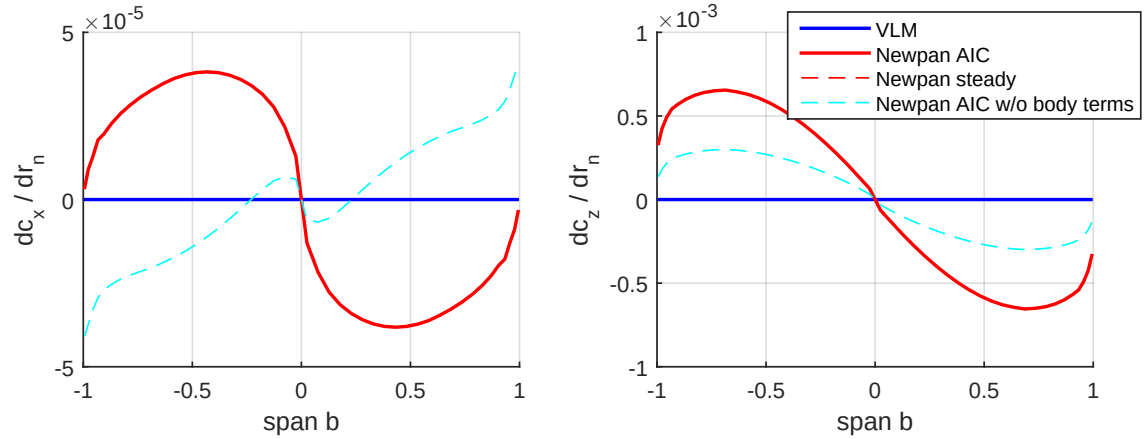

Figure 3: Drag and lift gradient distribution due yaw rate r_n.

the "classical" VLM is not able to capture any of these effects associated with beta. Integration of the lift over the span, yields the desired rolling moment coefficient C_{L_β}. To illustrate the importance of the additional terms in equation (8), the distributions without those terms are included as well.

Another effect is the yawing moment due to roll rate C_{N_p}. Lift and Drag distributions are shown in figure 2. The lift distribution is well captured by both potential flow methods. The forces in x-direction are induced by a change of angle of attack along the wing span due to the roll rate. Since the "classical" VLM does not capture the direction of lift, those forces are zero. In contrast, the panel method shows an distribution of the forces in x, however, somewhat lower when compared to the CFD results. The value for the yawing moment coefficient C_{N_p} is obtained by integration of the distribution over the span.

Unfortunately, there were no conclusive CFD results available for the yaw rate case . The distributions in figure 3 are therefore only useful for a qualitative statement. It should also be noted that for the chosen reference flight state at $\alpha = 0°$, the static loading is very low, since the wing is only slightly cambered. The lift distribution in figure 3 for the panel method shows an increase in lift for the advancing wing and a decrease for the receding, which yields the expected rolling moment due to yaw rate C_{L_r}.

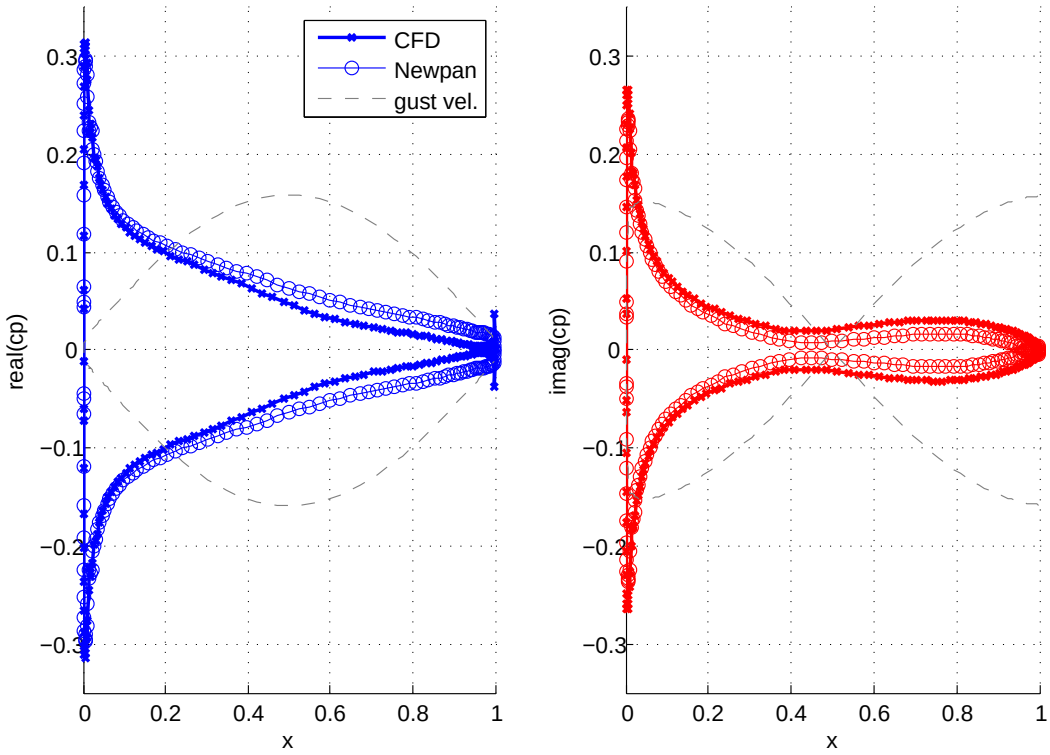

Figure 4: Complex pressure distribution of a symmetric airfoil due to a sinusoidal gust with $k_G = 1.5$.

2.3.2 Complex pressure distribution of airfoil due a sinusoidal gust

To validate the gust induced pressures a 2D airfoil test case was selected. For the CFD calculations a NACA64A010 airfoil was subjected to a sinusoidal gust excitation. Again a subsonic conditions were chosen ($Ma = 0.6$) and the gust frequency k_G was varied to simulate several gust lengths. In the time domain enough cycles were computed to ensure that any transients are decayed. A Fourier transform is applied to the surface pressures which are then compared to the 3D panel results. The model for the 3D panel method consisted of a high aspect ratio half wing with approximately the same chordwise discretization as the CFD mesh. Then the center section of the resulting complex pressures are compared to the CFD results. Figure 4) shows the complex gust velocities and pressure coefficients from the panel method as well as the Euler type CFD calculation. The left hand side depicts the real, the right hand side the imaginary parts. The results for the case of $k_G = 1.5$ compare excellently, for the real as well as the imaginary part of the pressure coefficients. The panel method Newpan accurately discribes the pressures related to gust excitations.

3 LATERAL GUST ANALYSIS AND DUTCH ROLL MODE

A flight mechanics model is typically assumed to have no additional flexible or aerodynamic lag states. The effects of flexibility are usually accounted for by the aerodynamic database through flexible contributions to the total derivatives of the aircraft. Hence, the model merely has the 12 rigid body states of the Newton Euler equation of motion. When an eigenvalue analysis of that model is performed the eigenvectors constitute the flight mechanical modes. For longitudinal motion these are the short period and the phugoid mode; for the lateral motion these are the roll subsidence, the spiral divergence, which are typically aperiodic, i.e. eigenvalues on the real axis, and the dutch roll mode which has a conjugated complex pair of eigenvalues. The dutch

roll mode can be described as a combination of directional and lateral oscillation of an aircraft. An anecdote tells that the name stems from dutch ice skaters on frozen canals, whose motion resemble that of the aircraft dutch roll mode. The aerodynamic derivatives contributing to the dutch roll mode are the rolling and yawing moments due to sideslip, yaw and roll rate. The dutch roll is generally considered undesirable and for large aircraft actively damped by a yaw damper function in the flight control laws. The following investigation however is carried out by open loop simulations, i.e. no flight control system is active, to emphasize the differences of the aerodynamic submodels.

The lateral discrete gust is one of the critical load conditions for the Vertical Tail Plane (VTP). One important aspect is the excitation of the dutch roll flight mechanical mode, which can to lead to significant loads due to the rigid body motion. Since, the DLM is not able to accurately account for aforementioned important aerodynamic derivatives, considerable improvements in the rigid body dynamics are expected with the use of the 3D panel method.

3.1 Aircraft configuration and Wing Dihedral

To investigate the flight mechanic effects in a lateral gust simulation, a high wing configuration with a T-tail was chosen. This type of configuration usually has the lowest frequency flexible modes associated with the T-tail, so a large impact on the VTP loads can be expected during the gust encounter. Contributing factors to the dutch roll mode are a low center of gravity and a small tail volume. Further, increasing the wing sweep and the dihedral are aggravating the situation. High wing aircraft usually have anhedral (negative dihedral), since they are already prone to dutch roll motion.

To examine the influence of the wing dihedral on the dutch roll behavior and in particular the differences between the DLM and the panel method, the following two parameter variations were studied.

1. The reference configuration (with wing anhedral) and
2. a configuration with 0° wing dihedral

The fuselage was not aerodynamically modelled by volumetric or cruciform shaped panels, to highlight the differences of the wing effects. To add the destabilizing effect of the fore fuselage, flat vertical panels were used to reduce the weathercock stability derivative C_{N_β}, which would otherwise significantly over predicted. The T-tail is modelled with flat panels for the DLM as well as for the panel method. The main focus is on comparing the aerodynamic spanwise distributions of the thick, volumetric wing of the 3D panel method figure 5(a) versus the thin flat mean surface model of the DLM figure 5(b).

3.2 Quasisteady lift distributions

The most important aerodynamic stability derivatives are the rolling and yawing moments due to lateral excitation. It proves more insightful to have a look at the spanwise lift distributions of the wing, rather than at the integrated total derivatives. The emmpenage and fuselage panels remain unchanged and only little effect due to change in induced flow is expected.

Figure 6 depicts the gradients of these distributions, wrt sideslip, roll and yaw rates for the reference configuration with anhedral. While not entirely accurate for convenience reasons, the

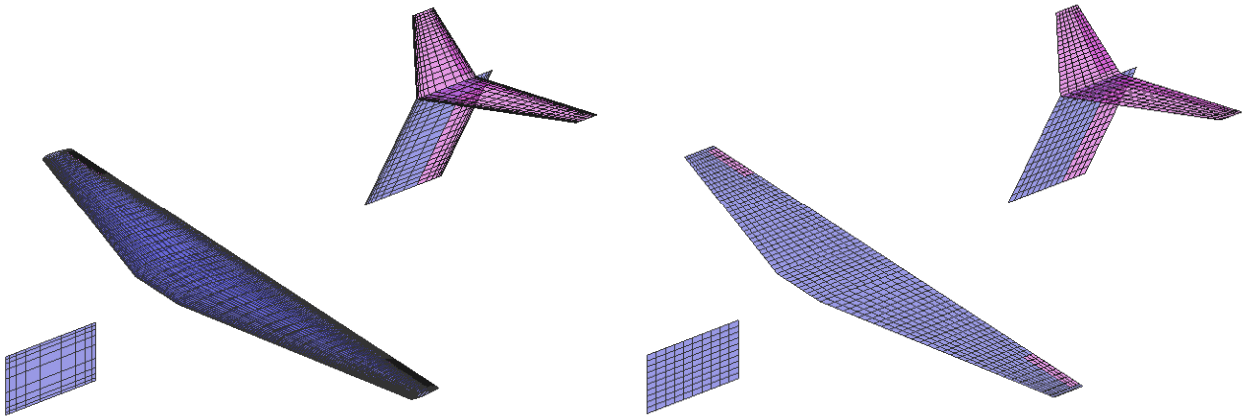

(a) Panel method grid (b) DLM grid

Figure 5: High wing T-tail configuration: aerodynamic grids

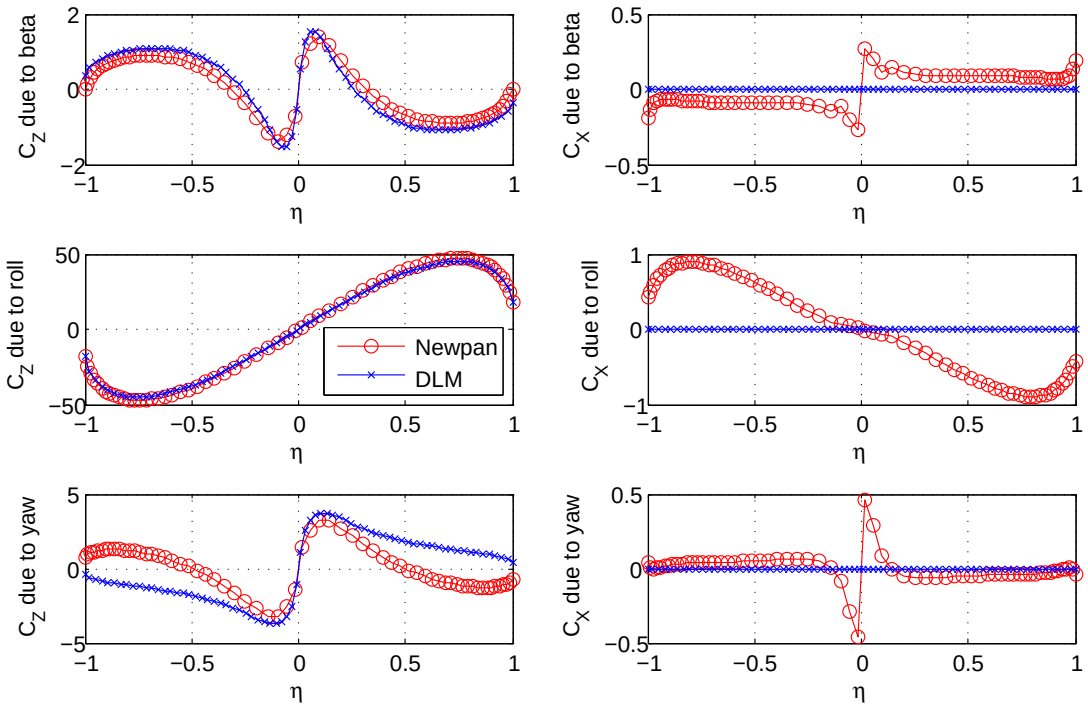

Figure 6: reference configuration with anhedral: lift and drag distribution due sideslip, roll and yaw rate

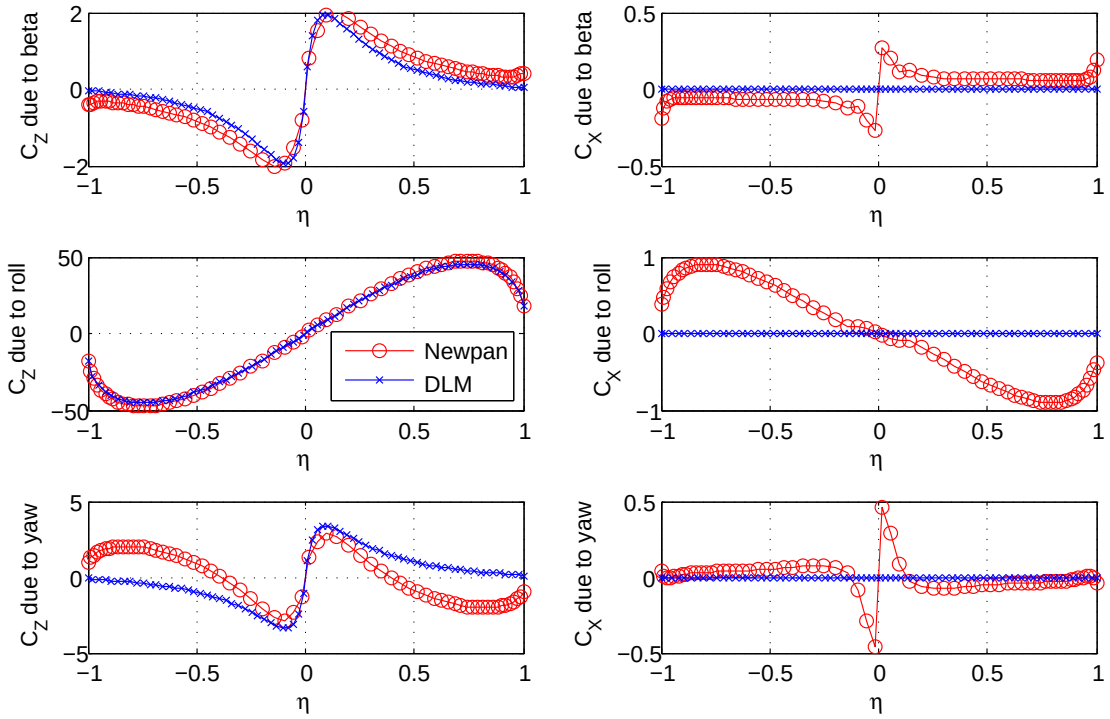

Figure 7: configuration with increased dihedral: lift and drag distribution due sideslip, roll and yaw rate

z-force will be named lift and the x-force will be called drag. First, the differences between DLM and Newpan are assessed:

When looking at the lift distributions a very good match is obvious for the sideslip and rolling motion. For the rolling motion this is to be expected, for the sideslip this comes somewhat as a surprise, since for the LANN wing (a wing only case with no dihedral), no lifting forces were produced by the DLM code, since no normalwash due to sideslip was induced on the flat panels. The yaw derivative shows differences due to the fact that the DLM does not account for an additional onset velocity due to the yaw rate. The qualitative trends are similar, nevertheless when integrating over the span, a significant rolling moment results for the DLM, in contrast to the panel method due to the sign change in the resulting lift distribution.

When comparing the drag forces major differences appear. Integrating the drag forces over the wing result in yawing moments which a completely absent for the DLM, due to the lack of forces in x-direction for the DLM. The change in lift direction due to the spanwise angle of attack change induced by the rolling motion and hence the missing yawing moment is only captured by Newpan. The same hold for the sideslip motion and less pronounced for the yaw rate.

Now the configuration is changed, and the anhedral is set to zero, which means effectively that this configuration has an increased dihedral. All distributions remain approximately the same, except for the lift distributions due to sideslip and yaw rate. The lift distributions due to yaw are shifted up consistently for DLM and Newpan. The more interesting change is visible for the lift distribution due to sideslip. Both, DLM and Newpan agree quite well, for the increased dihedral, the sign change in lift distributions disappears. Integration of the lift distribution due to beta over the wing, results in a restoring rolling moment. This is the expected behavior and is

the reason why C_{L_β} is sometimes also called the dihedral derivative. The increase of this value causes a more pronounced dutch roll mode.

3.3 Dutch roll mode

Next, the impact of these aerodynamic derivatives on the dutch roll mode are to be examined. To compute the flight mechanical eigenvalues a quasisteady model according to eq. (2) was set up. The first 20 structural modes with frequencies up to 10 Hz are included in the model. The model constitutes a non-linear system of ordinary differential equations with 52 states, 12 due to the nonlinear rigid body part of the equations of motion and 40 due to the 20 structural dynamic modes. Next, the aircraft model is trimmed for steady horizontal flight and linearized about this flight state. Now eigenvalues and eigenvectors are determined and the associated frequencies and damping values are computed. The dutch roll mode is identified and summarized for the different configurations in table 1. It should be noted that the lowest frequency structural mode is the T-Tail bending, which is at around 2 Hz, is also significantly participating in the dutch roll mode.

	reference config.		config. with increased dihedral	
	f	g	f	g
DLM	0.26692 Hz	0.21643	0.25723 Hz	0.20901
Newpan	0.26457 Hz	0.16639	0.25352 Hz	0.14851

Table 1: Dutch roll frequencies and damping for reference and increased dihedral configuration.

The frequencies for the DLM and the panel method are almost identical. However, there is a significantly reduced damping in the case of the 3D panel code. This can be attributed to the missing flight mechanical effects in the DLM. When the configuration with the increased dihedral is considered, the frequencies and damping is reduced. This is consistent for both aerodynamic methods. The reduction in damping for the panel method is more pronounced.

3.4 Lateral gust transfer functions

Now the question arises, how much influence the differences between the aerodynamic methods have on the lateral gust load results. To assess that a frequency domain gust loads calculation has been set up. The frequency domain gust equation is derived from the linear equations of motion (1), by solving for the generalized deformations $\mathbf{u}_h$. The gust equation then reads:

$$\left[-\omega^2\mathbf{M}_{hh} + \mathrm{j}\,\omega\mathbf{B}_{hh} + \mathbf{K}_{hh} - q_\infty\mathbf{Q}_{hh}(\omega)\right]\mathbf{u}_h(\omega) = q_\infty\mathbf{Q}_{hG}(\omega), \tag{14}$$

where $\mathbf{Q}_{hG}$ is the generalized AIC matrix for the gust input. To derive this matrix, the AIC matrix is multiplied with the vector of time delays to the individual panels, i.e. eq. (9) but without the specific gust spectrum $\mathbf{v}_G(\omega)$. Once solved for the transfer functions, results for different gust spectra can be calculated by simple matrix multiplications within seconds. Once the generalized deformations $\mathbf{u}_h(\omega)$ are computed, the loads are recovered with the force summation method:

$$\mathbf{P}_g(\omega) = \underbrace{q_\infty\left[\mathbf{Q}_{gG}(\omega) + \mathbf{Q}_{gh}(\omega)\mathbf{u}_h(\omega)\right]}_{\mathbf{P}_g^{\mathrm{ext}}} - \underbrace{\omega^2\mathbf{M}_{gh}\mathbf{u}_h(\omega).}_{\mathbf{P}_g^{\mathrm{iner}}} \tag{15}$$

Integration of the individual loads P_g along the structural component, leads to the internal cut loads, which the structure has to be sized against. Please note, that the subscript capital G refers to the gust, whereas g is the physical, structural degree of freedom set.

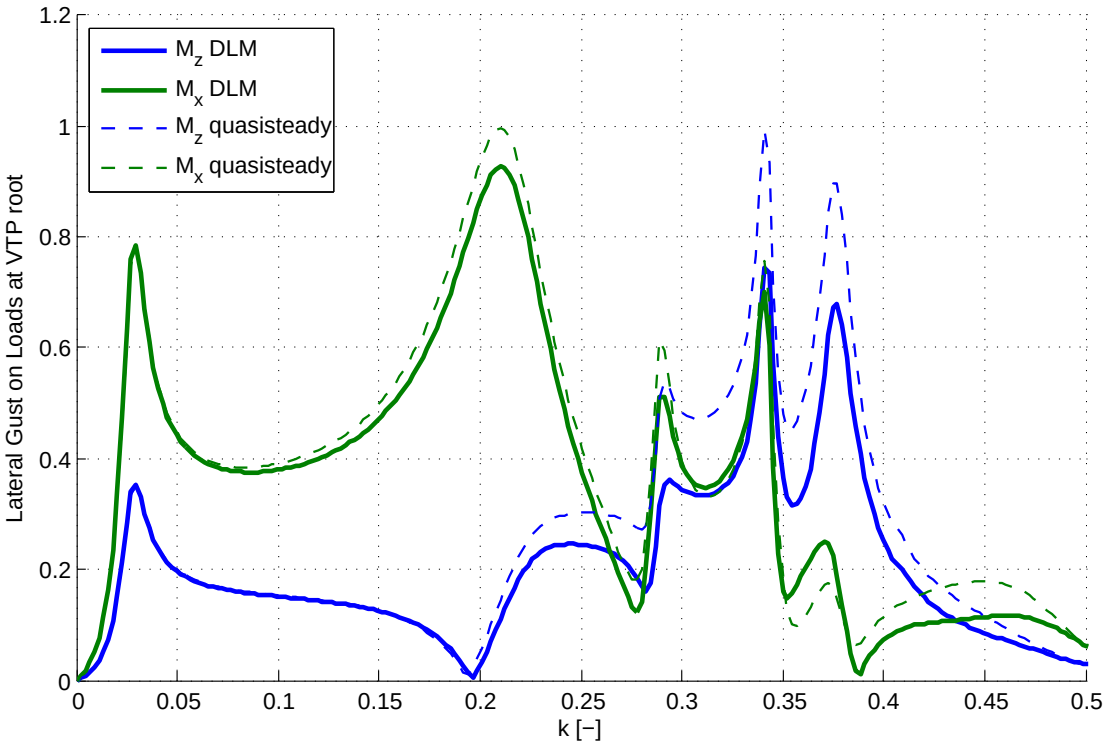

Figure 8: Transfer function: lateral gust input on VTP root bending and torsion moment for the DLM

The gust loads analysis is done for both aerodynamic methods. The examined loads are bending and torsion moment at the VTP root due to the lateral gust input, i.e. to get the resulting loads due to specific gust, a corresponding spectrum yet has to be postmultiplied, e.g. to assess the impact of different discret 1-cos gust gradient lengths or turbulence levels. Additionally a quasisteady approximation for the for both aerodynamic methods was used. This means the AIC matrix for the zero reduced frequency $\mathbf{Q}_{jj}(k = 0)$ is used for all frequency excitations. This is done to determine the effects of unsteady aerodynamics.

Figures 8 and 9 depict the absolute values for the mentioned load quantities. The phase diagram was ommitted. All loads shown in the graphs are normalized by the maximum occurring load for an easier comparison. The frequencies are expressed in terms of the unitless reduced frequency.

The first peak at the lowest frequency is the dutch roll. There the bending moment M_x and the torsion moment M_z correlate. Also note that in this low frequency case the quasisteady approximation is extremely accurate. The second peak in M_x, where the also the maximum is reached, occurs at the frequency of the first structural bending of the VTP. The highest peak for M_z happens at a higher freqency and is also correlated with a peak in bending moment M_x.

When comparing the DLM with the panel method, the similarity in shapes for the peaks and their associated frequencies are obvious. This is an expected result since the underlying structural model is the same and no a dramatic change in behaviour due to the two different aerodynamic methods was expected. Somewhat surprising is the sigificant lower loads level for the panel method compared to the DLM aerodynamics. Here further investigations are necessary, in particular a closer look at the actual T-tail aerodynamics deserves further scrutiny.

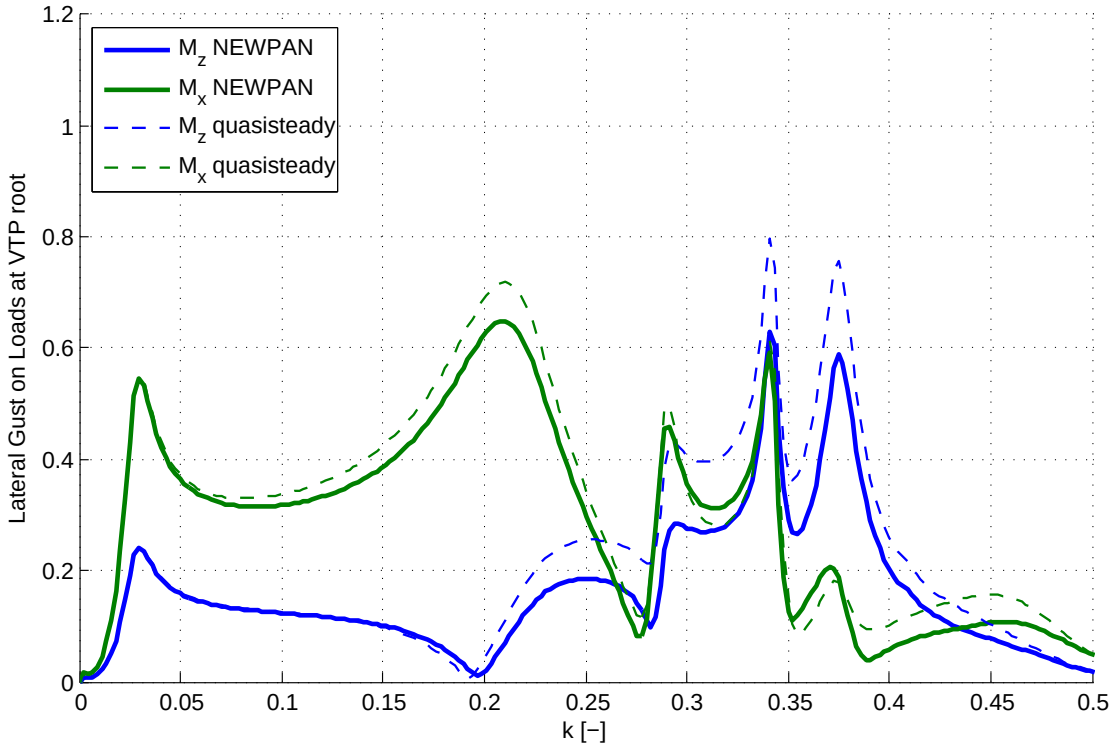

Figure 9: Transfer function: lateral gust input on VTP root bending and torsion moment for NEWPAN

Another observation that can be made, is that the levels of the higher frequency peaks for torsion and bending moment in relation to the first VTP bending mode are different. For the DLM the difference between the peaks is significantly higher for the DLM, whereas for the panel method they are almost the same magnitude. The peak at $k = 0.34$ for the bending almost reaches the maximum associated with the first structural VTP bending.

The reason for the mentioned differences in response warrants further investigations.

4 SUMMARY AND CONCLUSION

Previously, steady Aerodynamic Influence Coefficients (AICs) matrices of a 3D panel method were used for manoeuvre type simulations [7, 8]. In this paper the application of the panel method was significantly extended by using its AICs for an unsteady frequency domain gust loads analysis.

The process for loads analysis models integration with the AICs of the 3D panel method Newpan was outlined. First, the equations of motion for manoeuvre loads simulations, respectively linear frequency domain loads analyses were summarized. Then, the governing flow equations of the unsteady panel method were established and contrasted to the Doublet Lattice Method. Additional pressure terms necessary for panel method thick bodies were introduced in the boudary conditions for rigid body motion, flexible deformation and control surface deflections. A validation of the panel method was done by comparing quasi-steady lift and drag distributions with CFD calculations of the LANN wing. The panel method is able to model important flight mechanical effects that were not present with classical, DLM type AIC matrices. Next, the complex pressure distribution of a sinusoidal gust was compared to CFD calculations showing an excellent agreement, reassuring the suitability for the gust loads computation.

An aircraft configuration with a high wing and T-tail was chosen for a lateral gust loads analysis. This type of configuration is prone to the dutch roll mode, which may be excited by a lateral gust. Quasi-steady manoeuvre loads analysis models were set up to examine the effects of an increased wing dihedral for the panel method and the DLM. The impact of this parameter variation on the dutch roll frequency and damping was assessed for both aerodynamic methods.

A frequency domain gust loads analysis comparing DLM with 3D panel method results was carried out. The results are promising, although some differences between the methods were noticed. If they can be attributed solely to the previously missing coupling effects needs to be explored further. In particular a closer look on the T-tail aerodynamics is indicated, since similar effects to those associated with flight mechanics, might result in a difference of the loads response. T-tails are notoriously difficult to analyze with the DLM, due to the missing in plane aerodynamic effects [22].

In this paper, the Aerodynamic Influence Coefficients (AICs) of a 3D panel method were successfully used in the model integration for frequency domain gust loads analysis. Also the applicabilty in the context of manoeuvre loads and flight dynamics has been demonstrated. Additional aerodynamic effects directly influence e.g. the dutch roll dynamics, which were unaccounted for by the Doblet Lattice Method. As a next step, it is planned to use the panel method AICs for analyzing T-tail flutter behaviour and their impact on the flutter speed compared to the DLM.

5 REFERENCES

[1] Albano, E. and Rodden, W. (1969). A doublet-lattice method for calculating lift distributions on oscillating surfaces in subsonic flows. *AIAA Journal*, 7(2), 279–285. doi: 10.2514/3.5086 10.2514/3.55530.

[2] Rodden, W., Giesing, J., and Kalman, T. (1971). New developments and applications of the subsonic doublet-lattice method for nonplanar configurations. In *AGARD Symposium on unsteady aerodynamics for aeroelastic analyses of interfering surfaces*, AGARD-CP-80-71. AGARD.

[3] Rodden, W., Taylor, P., and Jr., S. M. (1998). Further refinement of the subsonic doublet-lattice method. *Journal of Aircraft*, 9(10), 693–702. doi:10.2514/2.2382.

[4] Kier, T. and Looye, G. (2009). Unifying Manoeuvre and Gust Loads Analysis. In *International Forum on Aeroelasticity and Structural Dynamics*, IFASD-2009-106.

[5] Hedman, S. (1965). Vortex Lattice Method for Calculation of Quasi Steady State Loadings on Thin Elastic Wings. Tech. Rep. Report 105, Aeronautical Research Institute of Sweden.

[6] Fiddes, S. P., Burkett, C. W., and Kier, T. M. (2015). An advanced panel method for compressible subsonic unsteady flow past complex geometries. In *International Forum on Aeroelasticity and Structural Dynamics*, IFASD-2015-181.

[7] Kier, T. M. (2015). Integrated flexible dynamic maneuver loads models based on aerodynamic influence coefficients of a 3d panel method. In *56th AIAA/ASCE/AHS/ASC Structures, Structural Dynamics, and Materials Conference, 5-9 January 2015, Kissimmee, FL, USA*, AIAA 2015-0185. AIAA. doi:10.2514/6.2015-0185.

[8] Kier, T. M., Verveld, M. J., and Burkett, C. W. (2015). Integrated flexible dynamic loads models based on aerodynamic influence coefficients of a 3d panel method. In *International Forum on Aeroelasticity and Structural Dynamics*, IFASD-2015-179.

[9] Hofstee, J., Kier, T., Cerulli, C., et al. (2003). A Variable, Fully Flexible Dynamic Response Tool for Special Investigations (VarLoads). In *International Forum on Aeroelasticity and Structural Dynamics*.

[10] Guyan, R. J. (1965). Reduction of stiffness and mass matrices. *Journal of Aircraft*, 3(2), 380. doi:10.2514/3.2874.

[11] Waszak, M. R. and Schmidt, D. K. (1986). On the flight dynamics of aeroelastic vehicles. In *AIAA Atmospheric Flight Mechanics Conference*, AIAA 86-2077. AIAA, pp. 120–133. doi:10.2514/6.1986-2077.

[12] M. R. Waszak and D. K. Schmidt (1988). Flight Dynamics of Aeroelastic Vehicles. *Journal of Aircraft*, 25(6), 563–571. doi:10.2514/3.45623.

[13] R. L. Bisplinghoff, H. Ashley, R. L. Halfman (1955). *Aeroelasticity*. Dover Publications Inc.

[14] Göthert, B. (1940). Ebene und räumliche Strömung bei hohen Unterschallgeschwindigkeiten: Erweiterung der Prandtl'schen Regel. Tech. Rep. Bericht 127, Lilienthal Gessellschaft.

[15] Roger, K. L. (1977). Airplane math modeling methods for active control design. In *AGARD Structures and Materials Panel*, AGARD/CP-228. AGARD, pp. 4–1 – 4–11.

[16] Edwards, J. W. (1979). Applications of Laplace transform methods to airfoil motion and stability calculations. In *20th Structures, Structural Dynamics and Materials Conference*, AIAA 1979-772. doi:10.2514/6.1979-772.

[17] Abel, I. (1979). An analytical technique for predicting the characteristics of a flexible wing equipped with an active flutter-suppression system and comparison with wind-tunnel data. Tech. Rep. NASA TP-1367, NASA LARC.

[18] Karpel, M. (1981). Design for Active and Passive Flutter Suppression and Gust Alleviation. Tech. Rep. NASA CR-3482, NASA.

[19] Harder, R. and Desmarais, R. (1972). Interpolation Using Surface Splines. *Journal of Aircraft*, 9(2), 189–191. doi:10.2514/3.44330.

[20] Rodden, W. P. and Johnson, E. H. (1994). *MSC.Nastran Aeroelastic Analysis User's Guide*. MSC.

[21] Malone, J. and Ruo, S. (1983). Lann wing test program: Acquisition and application of unsteady transonic data for evaluation of three-dimensional computational methods. Tech. Rep. AFWAL-TR-83-3006, Wright Lab., Wright-Patterson AFB.

[22] Murua, J., Martinez, P., Climent, H., et al. (2014). T-tail flutter: Potential-flow modelling, experimental validation and flight tests. *Progress in Aerospace Sciences*, 71, 54–84. doi:10.1016/j.paerosci.2014.07.002.

COPYRIGHT STATEMENT